

# Load Transfer and Deformation Characteristics of the Pelvis in Non-destructive Side Impact Testing

Andrew Kemper, Craig McNally, and Stefan Duma  
Virginia Tech – Wake Forest, Center for Injury Biomechanics  
United States of America  
Paper Number 09-0508

## ABSTRACT

Although finite element models of the human body are becoming an integral tool in the reduction of automobile related injuries, these models must be locally and globally validated to be considered accurate. Therefore, the purpose of this study was to quantify the load transfer and deformation characteristics of the pelvis in side impact loading. A total of ten non-destructive side impact tests were performed on two human male cadavers. Three impact areas and two impacting surfaces were evaluated using a 16 kg pneumatic impactor at approximately 3 m/s: rigid-impact to the ilium, rigid-impact to the greater trochanter, rigid-impact to the ilium and greater trochanter, and foam-impact to the ilium and greater trochanter. Additional rigid-impacts to the ilium and greater trochanter were performed on one cadaver at 4 m/s and 5 m/s to evaluate the effect of loading rate. Load transfer through the pelvis was quantified by implanting custom *in situ* pelvic load cells in the ilio-sacral joint and pubic symphysis joint. In addition, strain gages were applied to the iliac wing, superior pubic ramus, ischium, and femur. The results showed that for all test conditions, except the rigid-impact to the iliac crest, a larger percentage of impactor force was transferred through the pubic symphysis joint than the ilio-sacral joint. The strain gage data showed that for all test conditions except one, ilium only impact, the superior pubic ramus and ischium were placed in compression. Conversely, the primary loading mode for the ilium 1<sup>st</sup> principle strain was tension for all test conditions. Impact speed was not found to have a considerable affect on the distribution of load through the pelvis. It is anticipated that this research will further the understanding of the biomechanical response of the human pelvis in side impact loading, and aid in the development and validation of computational models.

## INTRODUCTION

The incidence of pelvic fractures in the United States is estimated to be more than 100,000 per year [9]. Motor vehicle collisions account for

44–64% of pelvic fractures, which are a major cause of death and residual disability in blunt trauma [6]. In addition, studies have shown that frontal occupants involved in lateral motor vehicle collisions have a significantly higher risk of sustaining a pelvic fracture versus those involved in a frontal collision [12, 13]. Understanding the biomechanical response of the pelvis to various loading conditions is the first step in reducing the number of incidences and severity of pelvic fractures. There have been a number studies which have investigated the biomechanical response and tolerance of the pelvis in lateral impact loading representative of that seen in motor vehicle side impact collisions [1, 2, 3, 4, 5, 11]. However, the injury criteria based on the results of these studies rely primarily on censored fracture data. Although finite element models of the human body are becoming an integral tool in the reduction of automobile related injuries, these models must be locally and globally validated in order to accurately predict injury. Therefore, the purpose of this study was to quantify the load transfer and deformation characteristics of the pelvis in side impact loading.

## METHODS

A total of 10 non-destructive side impact tests were performed on two fresh previously frozen human male cadavers. Subject information and pelvic anthropometric measurements from each cadaver were recorded (Table 1).

**Table 1:** Subject information.

Test Measurement		Cadaver ID	
		1	2
Age	(yr)	75	57
Weight	(kg)	65	84
Height	(cm)	165	177
Pelvis Length (anterior-posterior)	(mm)	165	172
Pelvis Width (medial-lateral)	(mm)	285	320
Pelvis Height (superior-inferior)	(mm)	190	220

**In Situ Pelvic Load Cells**

In order to quantify the load transfer through the pelvis, *in situ* pelvis loads cell were implanted in the ilio-sacral joint (Robert A. Denton, Inc. 7458FL, 8896 N, Rochester Hills, MI) and the pubic symphysis joint (Robert A. Denton, Inc. 7457FL, 8896 N, Rochester Hills, MI) (Figure 1). The appropriate size and shape of the *in situ* pelvis load cells and mating plates used to attached the potting cups were based on anthropometric measurements from 6 human pelvi (Figures 2 and 3). The load cells were attached to the mating plates with a dove-tail design. The dove-tail fixed the load cell in the medial-lateral direction, and set screws fixed the load cell in the anterior-posterior direction. The mating plates were designed to allow the load cell to be inserted from the anterior or posterior side of the post mortem human subject to allow for easy insertion and removal. This design provided a relatively simple attachment, while rigid enough to maintain the proper orientation.

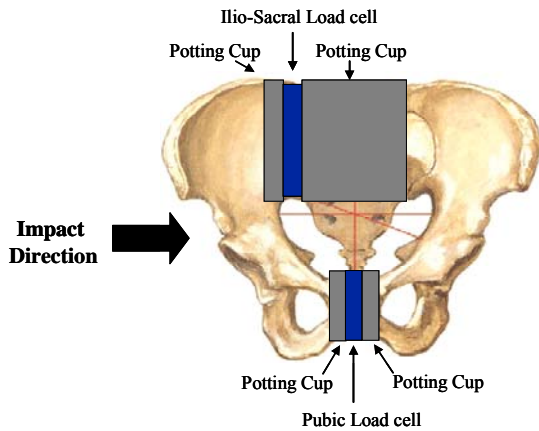


**Figure 1:** *In-situ* pelvic load cell locations.

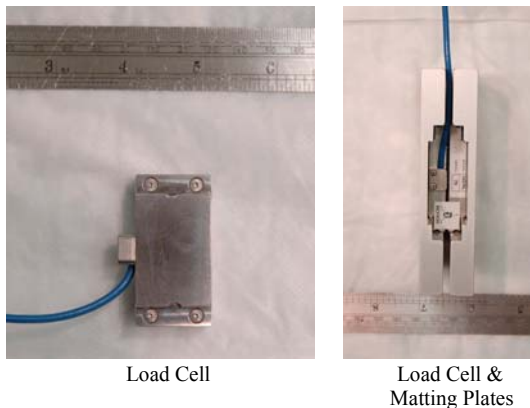


**Figure 2:** Pubic symphysis load cell.

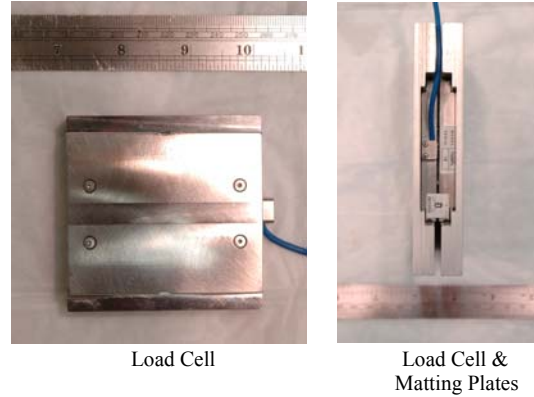


**Figure 3:** Ilio-sacral load cell.

The load cells were attached to the pelvis through a number of detailed steps. In order to preserve the normal orientation of the pelvis, the load cells were implanted one at a time. The ilio-sacral load cell was implanted first (Figure 4). This was done by first measuring the width of the pelvis, and then rigidly securing the pelvis to prevent movement during the process. Second, a section of bone was removed from the site insertion site, and a bone screw was placed through the ilium to provide a more rigid attachment when using the bonding compound. Third, potting cups and load cell were placed in the pelvis and positioned properly. Special care was taken to ensure that the measuring axis of the load cell was perpendicular to the sagittal plane. Then, the set screws were tightened to secure the load cell to the mating plates. The potting cups were then filled with a bonding compound (Bondo Corporation, Atlanta, GA), and bone screws were placed through the sacrum and L5. Finally, the pelvis width measurements were checked to ensure that they had not changed do the implantation of the ilio-sacral load cell.



**Figure 4:** Ilio-sacral load cell implantation.

Once the bonding compound for the ilio-sacral load cell fully cured, the pubic load cell was implanted (Figure 5). A section of bone was removed from the insertion site. Care was taken to leave the enough bone to maintain the connection between the upper and lower ramus. Third, the potting cups and load cell were placed in the pelvis and positioned properly. Again, special care was taken to ensure that the measuring axis of the load cell was perpendicular to the sagittal plane. Then, the set screws were tightened to secure the load cell to the mating plates. The potting cups were then filled with a bonding compound (Bondo Corporation, Atlanta, GA) and allowed to cure. Finally, the pelvic width measurements were rechecked to ensure that they had not changed do the implantation of the pubic load cell.



**Figure 5:** Pubic load cell implantation.

### Pelvic and Femur Strain Gages

Each cadaver was instrumented with 6 strain gages (Figure 6, Table 2). Single axis strain gages were applied along the main axis of the anterior portion of the superior pubic ramus and ischium. A strain gage rosette was placed on the interior portion of the ilium and was oriented towards the superior portion of the pelvis (Figure 7). The strain output from the three gages that composed each rosette was used to calculate the first and second principle strains. The first and second principle strains are calculated with the following equation (Equation 1). A single axis strain gage was applied to the lateral portion of the femur, aligned with the long axis, at the midpoint between the knee and hip. All strain gages were applied to the impacted side of the body.

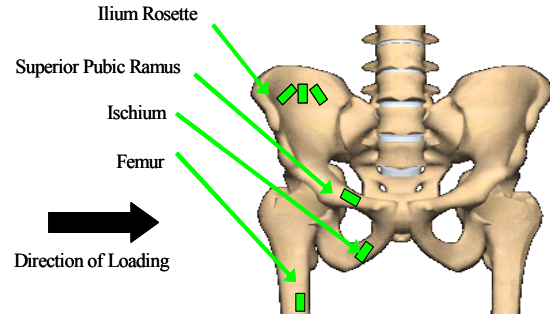


**Figure 6:** Strain gage locations for non-destructive side impact testing.

**Table 2:** Locations of strain gages and femur accelerometer.

Test Measurement Location		Cadaver ID	
		1	2
Ilium Rosette (to anterior superior iliac spine)	(mm)	57	50
Ilium Rosette (to posterior superior iliac spine)	(mm)	51	40
Pubic Ramus Gage (to pubic symphysis)	(mm)	52	50
Ischium Gage (to pubic symphysis)	(mm)	54	60
Right Femur Gage- (to center to patella)	(mm)	185	170

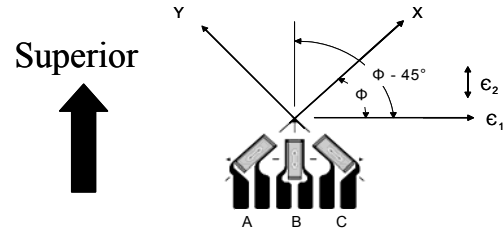


**Figure 7:** Ilium strain gage rosette labeling and orientation.

$$\epsilon_{1,2} = \frac{\epsilon_A + \epsilon_C}{2} \pm \frac{1}{\sqrt{2}} \sqrt{(\epsilon_A - \epsilon_B)^2 + (\epsilon_B - \epsilon_C)^2} \quad \text{Eqn (1)}$$

Where:

$\epsilon_A$  = Strain output from gage A of the rosette

$\epsilon_B$  = Strain output from gage B of the rosette

$\epsilon_C$  = Strain output from gage C of the rosette

### Experimental Setup

The primary component of the side impact experimental setup was a custom pneumatic impactor, which accelerates an impacting cart constrained by rails, to the desired speed via a piston (Figure 8). Prior to impact the piston loses contact with the cart, due to a limited piston stroke, resulting in an impact with finite energy. The displacement of the impacting cart, i.e. impactor stroke, was limited via a steel cable with a set length. The impactor was instrumented with a five-axis load cell (Robert A. Denton, Inc. 1968, 22,240 N, Rochester Hills, MI) and a single-axis accelerometer (Endevco 7264B, 2000 G, San Juan Capistrano, CA).

A custom test seat was designed and fabricated to allow a cadaver to be placed in a seated position (Figure 9). The use of an adjustable back support bar allowed for a clear line of sight to the posterior side of the cadaver, while maintaining an automotive-like seated posture and upper body load on the pelvis and spine. The head was held upright with the use of masking tape placed around the forehead and attached to the bar on the right and left side of the cadaver. This tape was cut approximately

half way though on both sides in order to ensure the tape would break once the cadaver was impacted. A Teflon<sup>®</sup> sheet was placed between the cadaver and the seat pan to minimize friction [2].

During the impact, the impactor plate contacted a trigger strip that was secured to the outermost portion of the pelvis to activate the data acquisition system for each test. Data from the load cell and strain gages were recorded at a sampling frequency of 15 kHz with an Analog-to-Digital conversion resolution of 16 bits using an Iotech Wavebook with WBK16 strain gage modules (Iotech WBK16, Cleveland, OH). Two high speed video cameras recorded the event from different angles (front and back view) at 1000 fps. All channels except for the strain gages were filtered to Channel Filter Class (CFC) 180. The inertially compensated impactor force was calculated by summing the measured impactor force and inertial force. The inertial force was calculated by taking the product of the impactor acceleration and effective impactor mass, i.e. the impacting plate mass plus  $\frac{1}{2}$  the load cell mass.

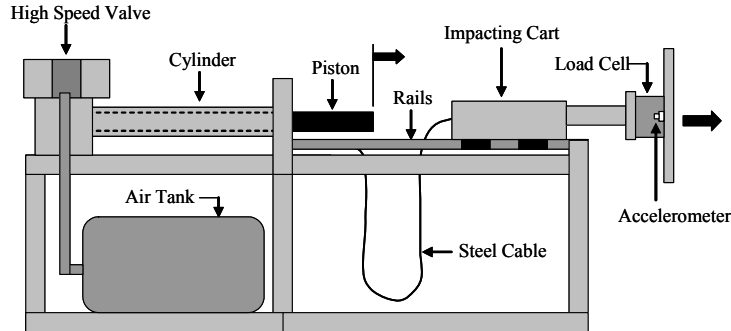


Figure 8: Custom pneumatic impactor.

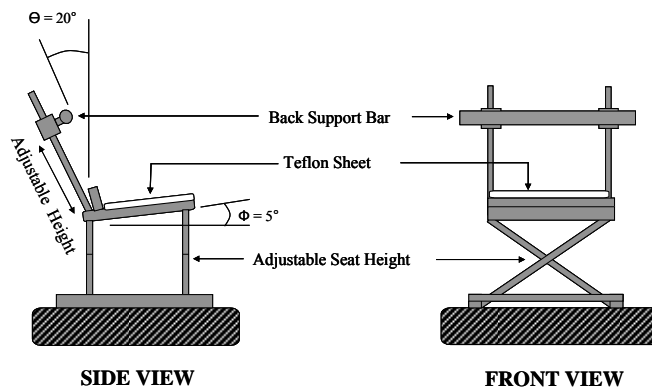


Figure 9: Custom side impact test seat.

**Impact Conditions**

A total of 10 non-destructive side impact tests were performed on two human male cadavers with a pneumatic impactor. Three impact locations and two impacting surfaces, rigid or foam, were evaluated (Table 3 and Figure 10). The combined ilium and femur impacts were performed with a 250 x 250 square impacting surface. In order to avoid contacting the testing seat, the square impactor was oriented at 22 degrees from horizontal. The ilium only impact and the trochanter only impact were performed using a rigid 127 mm diameter circular impacting surface. The majority of the testing was conducted at an impact speed of 3 m/s. However, two tests were performed on subject 2 higher impact velocities, 4 m/s and 5 m/s, to investigate the effects of loading rate. The impactor mass was 16 kg for all tests.

**Table 3:** Non-destructive pelvic side impact test summary.

Cadaver ID	Impact Surface	Impact Location	Speed
1	Foam	Ilium/ Femur	3 m/s
1	Rigid	Ilium/ Femur	3 m/s
1	Rigid	Ilium	3 m/s
1	Rigid	Trochanter	3 m/s
2	Foam	Ilium/ Femur	3 m/s
2	Rigid	Ilium/ Femur	3 m/s
2	Rigid	Ilium	3 m/s
2	Rigid	Trochanter	3 m/s
2	Rigid	Ilium/ Femur	4 m/s
2	Rigid	Ilium/ Femur	5 m/s

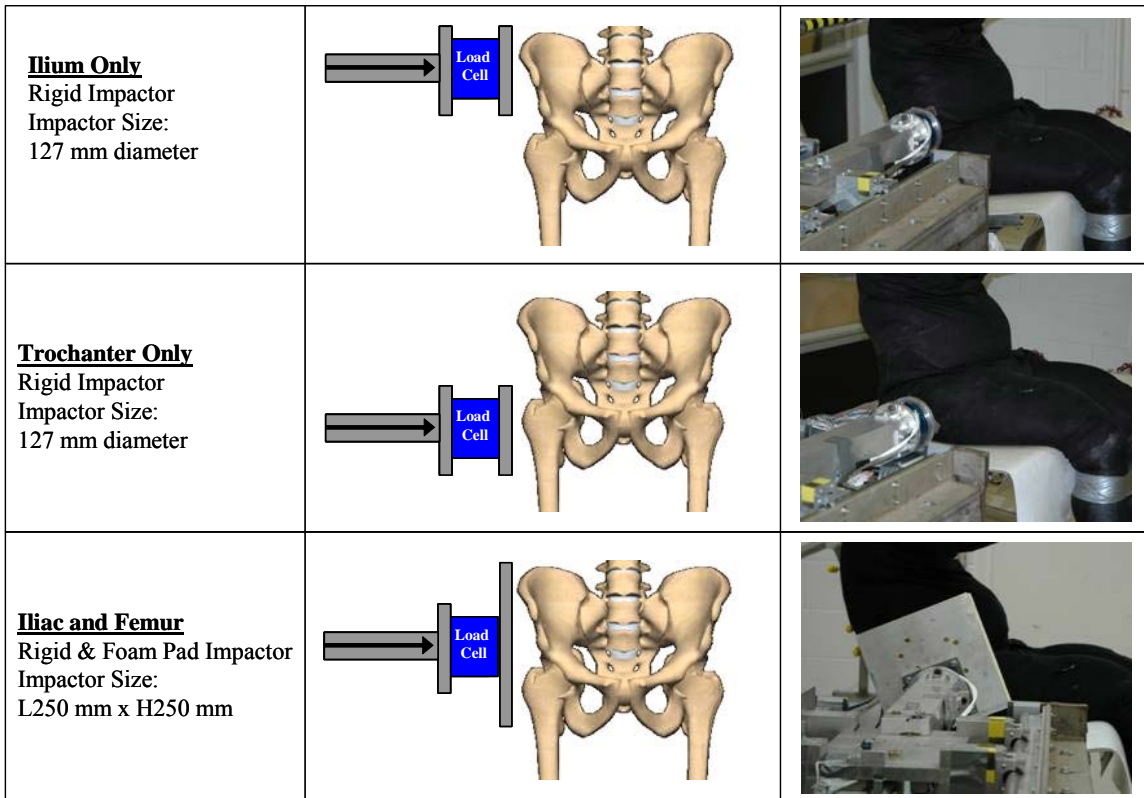


**Figure 10:** Impact locations and impactor surfaces.

## RESULTS

The results of the *in situ* pelvic load cells as well as the pelvic and femur strain gages are presented in this section. It should be noted that no pelvic or femoral fractures were observed as a result of these tests.

### Impactor Force and Pelvic Load Distribution

Each of the 10 non-destructive pelvic impact tests resulted in force time history for the impactor load cell, ilio-sacral load cell, and pubic load cell (Figure 11). The force time histories for each test are presented in the Appendix (Figures A1-A10). The reported impactor force is the inertially compensated impactor force. In

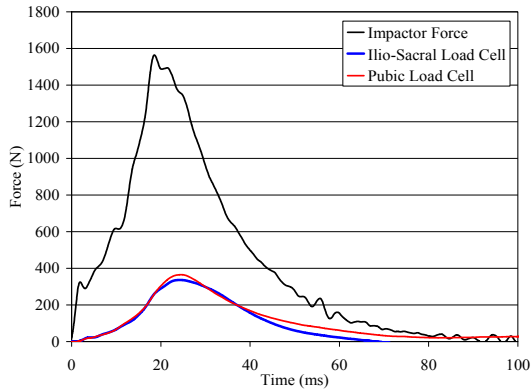


**Figure 11:** Typical force vs. time trace. (Cadaver 1- Ilium and femur - foam pad - 3m/s)

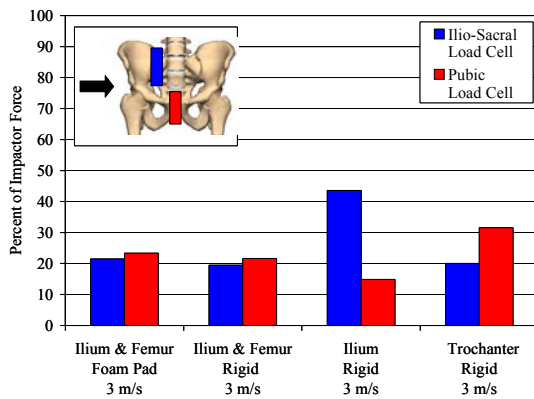


**Figure 12:** Cadaver 1 peak pelvic loads by test condition.

order to directly compare the load distribution through the pelvis for the different test conditions, the peak ilio-sacral load and peak pubic load are shown as a percentage of the peak impactor force (Figures 12-14). The peak impactor force, peak ilio-sacral force, and peak pubic force for each test are reported in Table 4.

### Pelvic Strain Distribution

The peak superior pubic ramus strain, ischium strain, femur strain, ilium 1<sup>st</sup> principle strain, and ilium 2<sup>nd</sup> principle strain in the primary mode of loading were plotted by test condition (Figures 15-17). The strain time histories for each test are presented in the Appendix (Figures A11-A20).

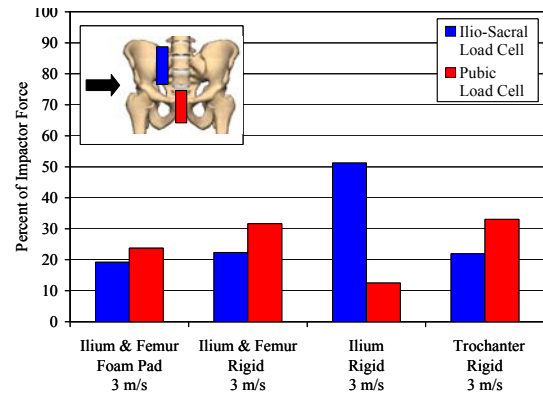


**Figure 13:** Cadaver 2 peak pelvic loads by test condition.

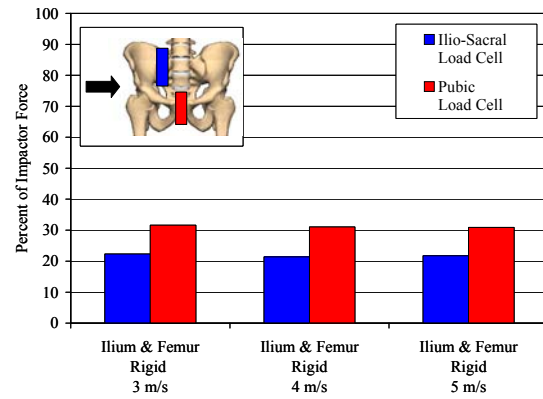


**Figure 14:** Cadaver 2 peak pelvic loads by loading rate.

**Table 4:** Peak impactor, ilio-sacral, and pubic forces.

Cadaver ID	Impact Location	Impactor Surface	Impact Speed	Peak Impactor Force	Peak Ilio-Sacral Force	Peak Pubic Force
				N	N	N
1	Ilium & Femur	Foam	3 m/s	1564	336	365
1	Ilium & Femur	Rigid	3 m/s	1654	322	358
1	Ilium	Rigid	3 m/s	1627	708	242
1	Trochanter	Rigid	3 m/s	1590	318	501
2	Ilium & Femur	Foam	3 m/s	1450	278	344
2	Ilium & Femur	Rigid	3 m/s	3100	693	980
2	Ilium	Rigid	3 m/s	2910	1490	363
2	Trochanter	Rigid	3 m/s	2982	654	986
2	Ilium & Femur	Rigid	4 m/s	4211	900	1307
2	Ilium & Femur	Rigid	5 m/s	6162	1340	1903

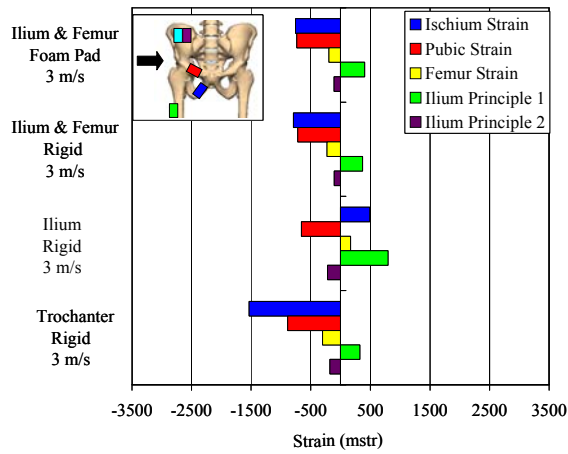


**Figure 15:** Cadaver 1 peak strain measurements. (primary mode of loading)

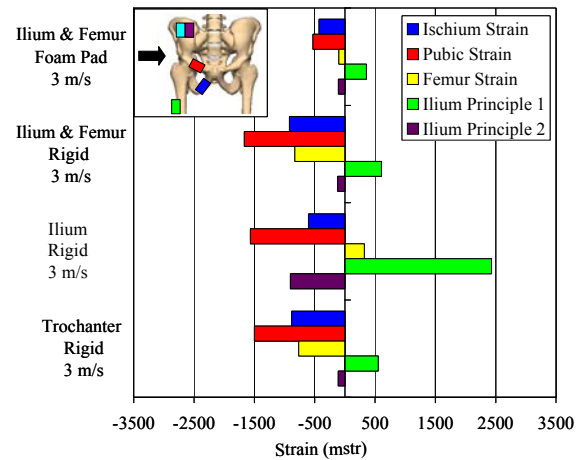


**Figure 16:** Cadaver 2 peak strain measurements. (primary mode of loading)

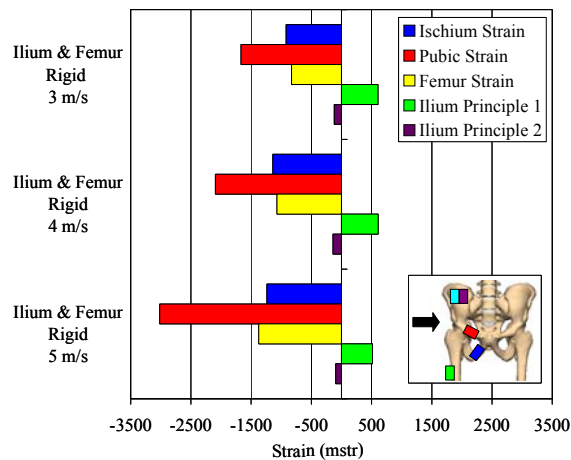


**Figure 17:** Cadaver 2 peak strain measurements by loading rates. (primary mode of loading)

## DISCUSSION

The *in situ* load cell data showed that the only test condition that resulted in a larger percentage of the impactor load through the ilio-sacral joint than the pubic symphysis joint was when only the ilium was impacted. In all other test conditions, the pubic symphysis joint received a larger percentage of the impactor load than the ilio-sacral joint. In addition, the force time histories show that for all tests except the ilium only impact the pubic symphysis and ilio-sacral joints are essentially loaded simultaneously. The higher velocity tests performed on Cadaver 2 showed that impact speed did not have any considerable effect on the load distribution through the pelvis. Finally, the results show that for every test a considerable amount of the impactor force was lost; i.e. not transmitted through the pelvis, due to the inertia of the body.

In the current study, the strain distribution of the pelvis was quantified with the use of *in situ* strain gages. The strain gage data showed that for all test conditions both the superior pubic ramus and ischium were placed in compression. Although the primary mode of loading for the ischium during the ilium only impact was tension, the ischium was initially placed in compression (Figure A13). In addition, the strain time histories show that for all tests except the cadaver 1 ilium only impact the superior pubic ramus was loaded before the ischium. This is due to the fact that the superior pubic ramus is directly attached to the acetabulum and the main axis of the superior pubic ramus is relatively close to orientation of the applied load. Therefore, the geometry of the pelvis relative to the loading axis resulted in a lag in the loading of the inferior pubic ramus. The primary loading mode for the ilium 1<sup>st</sup> principle strain was tension for all test conditions, while primary loading mode for the ilium 2<sup>nd</sup> principle strain was compression for all test conditions. The only test condition which resulted in a tension load on the lateral side of the femur was when only the ilium was impacted. In all other test conditions, the femur was in compression. The higher velocity tests performed on Cadaver 2 showed that all strain measurements except the ilium 1<sup>st</sup> and 2<sup>nd</sup> principle strains increased with increasing impact speed.

## CONCLUSIONS

In the current study the load transfer and deformation characteristics of the pelvis in side impact loading was quantified through 10 non-destructive tests performed on two human male cadavers. The results show that the only test condition which resulted in a larger percentage of the impactor load through the ilio-sacral joint than the pubic joint was when only the ilium was impacted. In all other test conditions, the pubic symphysis joint received a larger percentage of the impactor load than the ilio-sacral joint. The higher velocity tests performed on Cadaver 2 showed that impact speed did not have any considerable effect on the load distribution through the pelvis. For all tests a considerable amount of the impactor force was lost; i.e. not transmitted through the pelvis, due to the inertia of the body. With respect to pelvic strain, the results show that for all test conditions the superior pubic ramus and ilium 2<sup>nd</sup> principle strain were in compression. For all tests except one, a compressive load was placed on the ischium. Conversely, primary loading mode for the ilium 1<sup>st</sup> principle strain was tension for all test conditions. The only test condition which resulted in a tension load on the lateral side of the femur was when only the ilium was impacted. In all other test conditions, the lateral side of femur was placed in compression. The higher velocity tests performed on Cadaver 2 showed that ischium strain, superior pubic ramus strain, and femur strain increased with increasing impact speed. It is anticipated that this research will further the understanding of the biomechanical response of the human pelvis in side impact loading, and aid in the development and validation of computational models.

## ACKNOWLEDGEMENTS

The authors would like to thank Toyota Motor Corporation for providing the funding for this research.

## REFERENCES

- [1] D. Beason, G. Dakin, R. Lopez, , J. Alonso, F. Bandak, and A. Eberhardt, "Bone mineral density correlations with fracture load in experimental side impacts of the pelvis," *J. Biomechanics*, Vol. 36, pp. 219-217. 2003.
- [2] R. Bouquet, and M. Ramet, "Thoracic and pelvis human responses to impact," *Proc.*

- 14<sup>th</sup> International Conference on Enhanced Safety of Vehicles, Munich, Germany, 1994.
- [3] R. Bouquet, M. Ramet, F. Bermond, Y. Caire, Y. Talantikite, S. Robin, and E. Voiglio, "Pelvis human responses to lateral impact," *Proc. 16<sup>th</sup> International Conference on Enhanced Safety of Vehicles*, Windsor, Ontario, Canada, 1998.
- [4] J. Cavanaugh, Y. Haung, Y. Zhu, and A. King, "Regional tolerance of the shoulder, thorax, abdomen and pelvis to padding in side impact," *Society of Automotive Engineers Transactions*, Paper Number 930435, 1993.
- [5] D. Césari, and M. Ramet, "Pelvic tolerance and protection criteria in side impact," *Proc. 26<sup>th</sup> Annu. Stapp Car Crash Conference*, SAE 1982.
- [6] K. Inaba, P. Sharkey, D. Stephen, D. Redelmeier, F. Brenneman, "The increasing incidence of severe pelvic injury in motor vehicle collisions," *Injury*, vol. 35(8), pp. 759-765. 2004.
- [7] A. Kemper, C. McNally, E. Kennedy, A. Rath, S. Manoogian, J. Stitzel, S. and Duma, "Material properties of human rib cortical bone from dynamic tension coupon testing," *Stapp Car Crash Journal*, vol. 49, pp. 199-230. 2005.
- [8] A. Kemper, C. McNally, C. Pullins, L. Freeman, and S. Duma, "The biomechanics of human ribs: Material and structural properties from dynamic tension and bending tests," *Stapp Car Crash Journal*, vol. 51, pp. 235-273. 2007.
- [9] P. Rice, and R. Rudolph, "Pelvic Fractures," *Emergency Medicine Clinics of North America*, vol. 25(3), pp. 795-802. 2007.
- [10] S. Rouhana, P. Bedewi, S. Kankanala, P. Prasad, J. Zwolinski, A. Meduvsky, J. Rupp, T. Jeffreys and L. Schneider, "Biomechanics of 4-p seat belt systems in frontal impacts," *Stapp Car Crash Journal*, vol. 47, pp. 367-399. 2003.
- [11] D. Viano, I. Lau, and C. Asbury, "Biomechanics of the human chest, abdomen, and pelvis in lateral impact," *Accid. Anal. & Prev.*, vol. 21(6), pp. 553-574. 1989.
- [12] D. Stein, J. O'Connor, J. Kufera, S. Ho, P. Dischinger, C. Copeland, , and T. Scalea, "Risk factors associated with pelvic fractures sustained in motor vehicle collisions involving newer vehicles," *J. Trauma*, vol. 61(1), pp. 21-30. 2006.
- [13] E. Gokcen, A. Burgess, J. Siegel, S. Mason-Gonzalez, P. Dischinger, and S. Ho, "Pelvic fracture mechanism of injury in vehicular trauma patients," *J. Trauma.*, vol. 36(6), pp.789-95. 1994.

## Appendix

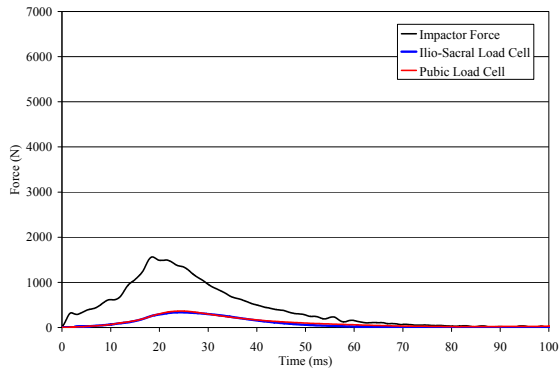


**Figure A1:** Cadaver 1 force vs. time (ilium and femur - foam pad - 3m/s)

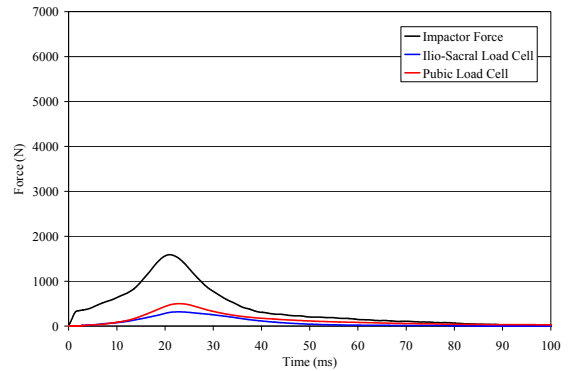


**Figure A4:** Cadaver 1 force vs. time (trochanter - rigid - 3m/s)

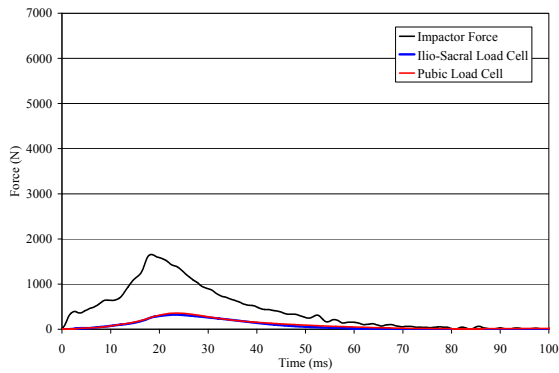


**Figure A2:** Cadaver 1 force vs. time (ilium and femur - rigid - 3m/s)

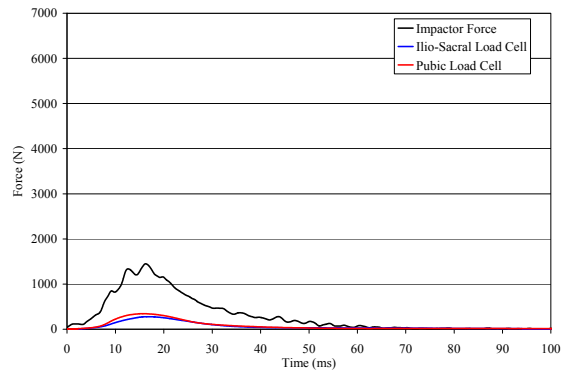


**Figure A5:** Cadaver 2 force vs. time (ilium and femur - foam pad - 3m/s)

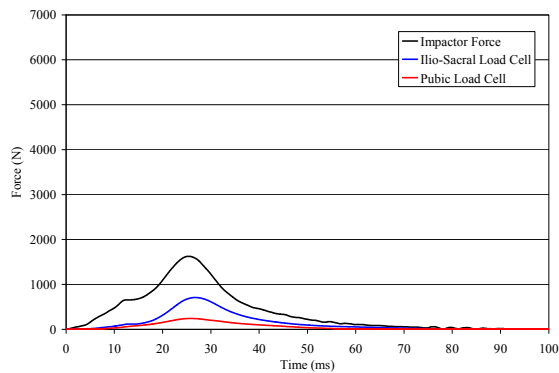


**Figure A3:** Cadaver 1 force vs. time (ilium - rigid - 3m/s)

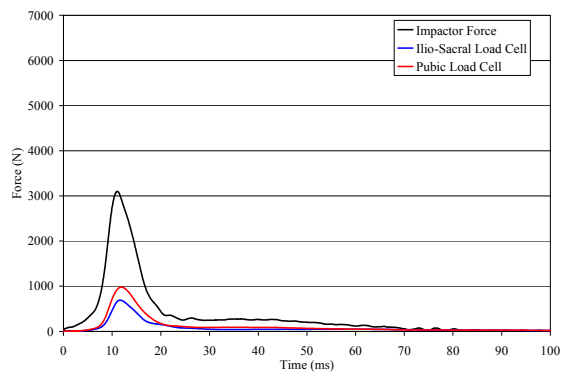


**Figure A6:** Cadaver 2 force vs. time (ilium and femur - rigid - 3m/s)

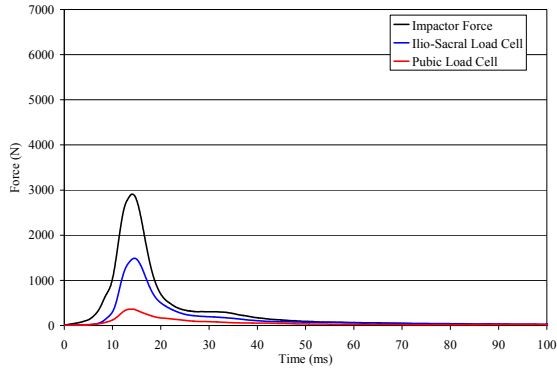


**Figure A7:** Cadaver 2 force vs. time  
(ilium - rigid - 3m/s)

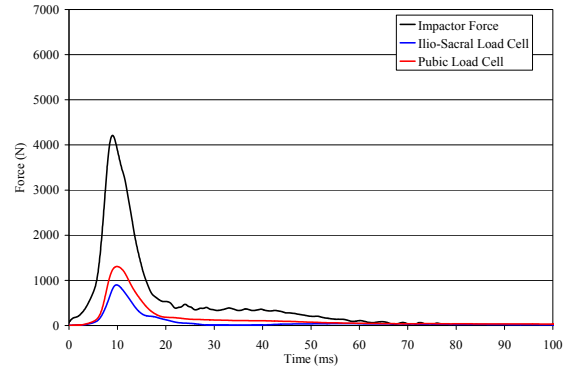


**Figure A9:** Cadaver 2 force vs. time  
(ilium and femur - rigid - 4m/s)

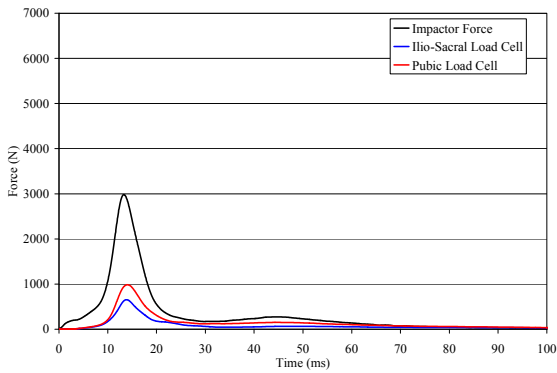


**Figure A8:** Cadaver 2 force vs. time  
(trochanter - rigid - 3m/s)

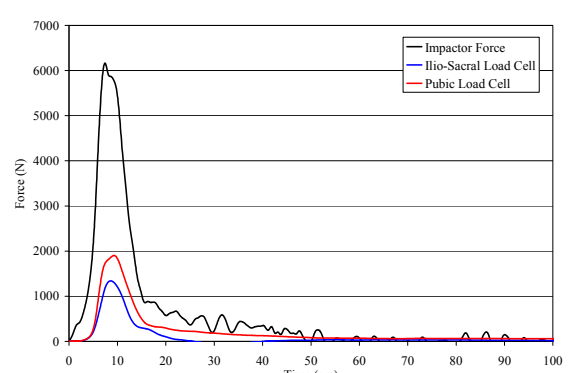


**Figure A10:** Cadaver 2 force vs. time  
(ilium and femur - rigid - 5m/s)

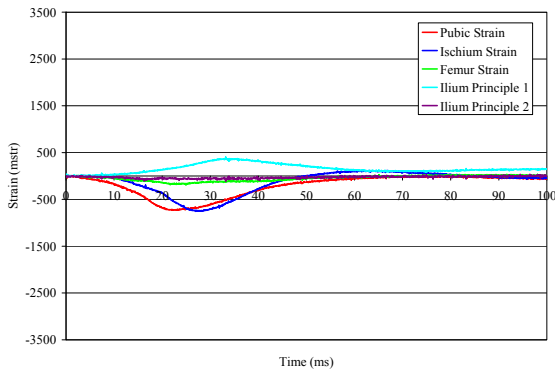


**Figure A11:** Cadaver 1 strain vs. time (ilium and femur - foam pad - 3m/s)

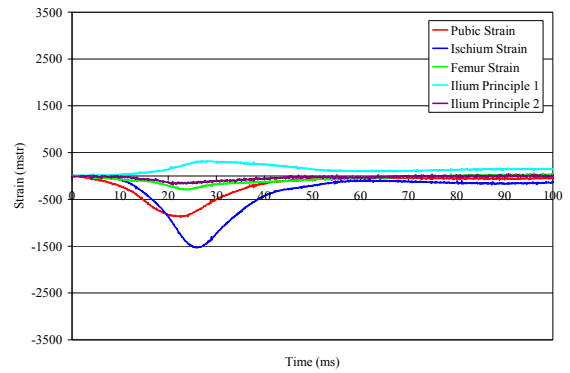


**Figure A14:** Cadaver 1 strain vs. time (trochanter - rigid - 3m/s)

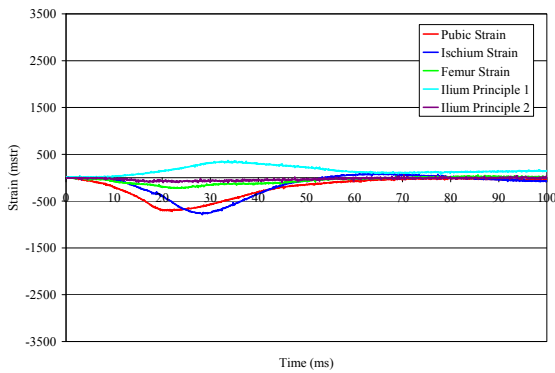


**Figure A12:** Cadaver 1 strain vs. time (ilium and femur - rigid - 3m/s)

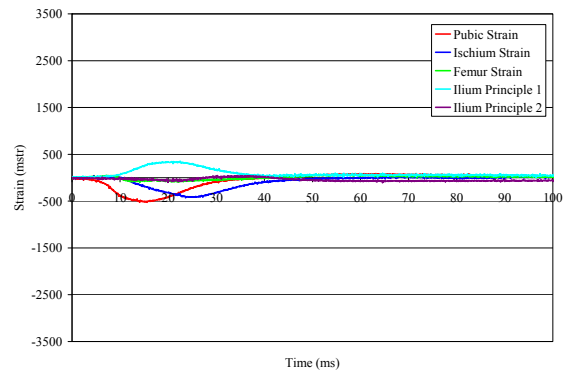


**Figure A15:** Cadaver 2 strain vs. time (ilium and femur - foam pad - 3m/s)

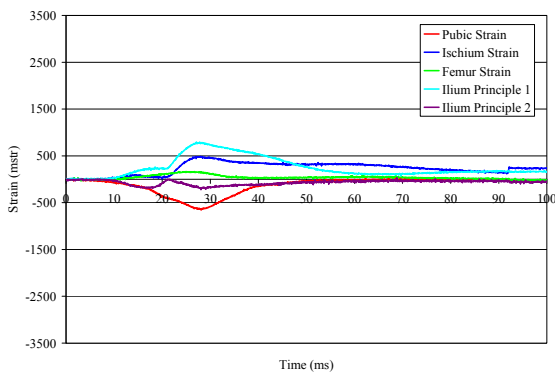


**Figure A13:** Cadaver 1 strain vs. time (ilium - rigid - 3m/s)

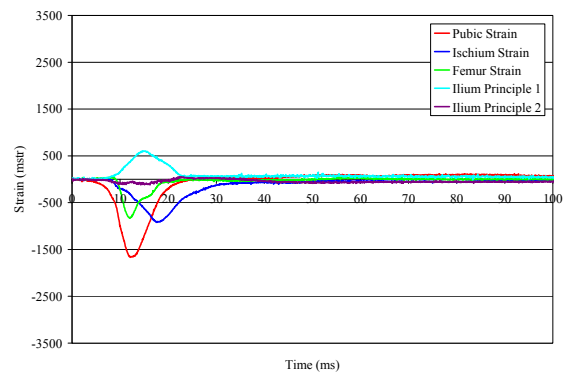


**Figure A16:** Cadaver 2 strain vs. time (ilium and femur - rigid - 3m/s)

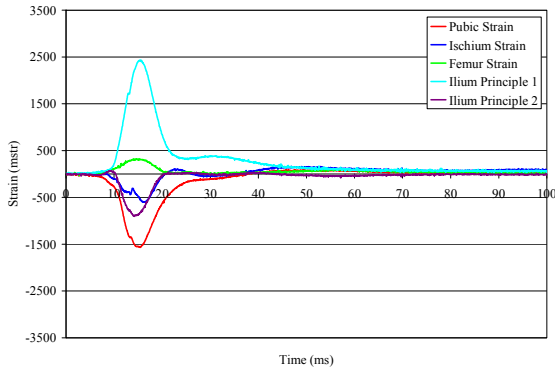


**Figure A17:** Cadaver 2 strain vs. time (ilium-rigid - 3m/s)

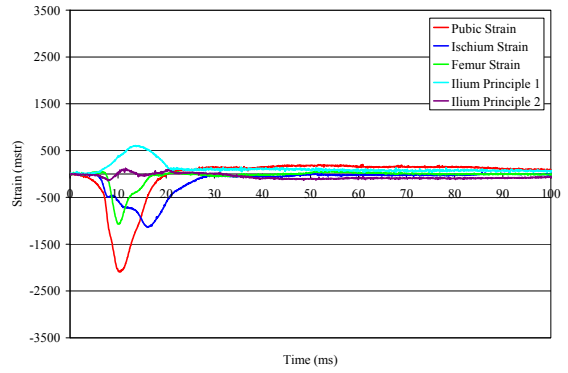


**Figure A19:** Cadaver 2 strain vs. time (ilium and femur - rigid - 4m/s)

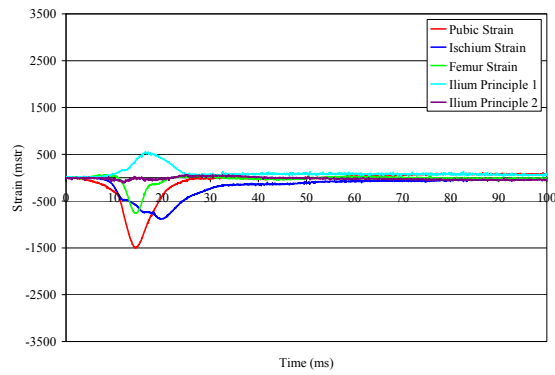


**Figure A18:** Cadaver 2 strain vs. time (trochanter - rigid - 3m/s)

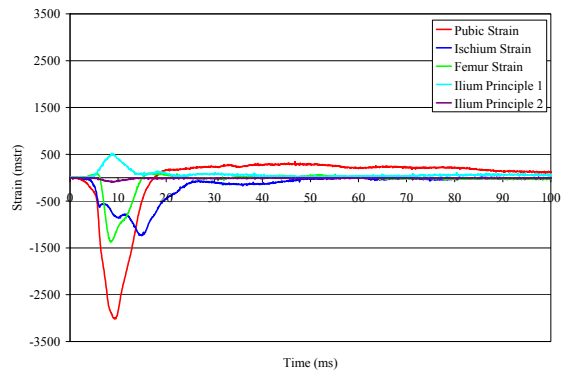


**Figure A20:** Cadaver 2 strain vs. time (ilium and femur - rigid - 5m/s)